

# Anisotropic dressing of charge-carriers in the electron-doped cuprate superconductor $\text{Sm}_{1.85}\text{Ce}_{0.15}\text{CuO}_4$ from angle-resolved photoemission measurements

A. F. Santander-Syro,<sup>1,2</sup> T. Kondo,<sup>3</sup> J. Chang,<sup>4</sup> A. Kaminski,<sup>3</sup> S. Pailhes,<sup>4,5</sup>  
M. Shi,<sup>6</sup> L. Patthey,<sup>6</sup> A. Zimmers,<sup>7</sup> B. Liang,<sup>7</sup> P. Li,<sup>7</sup> and R. L. Greene<sup>7</sup>

<sup>1</sup>Laboratoire Photons Et Matière, UPR-5 CNRS,

ESPCI, 10 rue Vauquelin, 75231 Paris cedex 5, France

<sup>2</sup>Laboratoire de Physique des Solides, UMR-8502 CNRS, Université Paris-Sud, 91405 Orsay, France

<sup>3</sup>Ames Laboratory and Department of Physics and Astronomy, Iowa State University, Ames, IA 50011

<sup>4</sup>Laboratory for Neutron Scattering, ETH Zurich and Paul Scherrer Institute, CH-5232 Villigen PSI, Switzerland

<sup>5</sup>Laboratoire Leon Brillouin, CEA-CNRS, CEA-Saclay, 91191 Gif-sur-Yvette, France

<sup>6</sup>Swiss Light Source, Paul-Scherrer Institut, CH-5232 Villigen, Switzerland and

<sup>7</sup>Center for Nanophysics and Advanced Materials,

Department of Physics, University of Maryland, College Park, MD 20742

(dated: February 21, 2024)

Angle-resolved photoemission measurements on the electron-doped cuprate  $\text{Sm}_{1.85}\text{Ce}_{0.15}\text{CuO}_4$  evidence anisotropic dressing of charge-carriers due to many-body interactions. Most significantly, the scattering rate along the zone boundary saturates for binding energies larger than 200 meV, while along the diagonal direction it increases nearly linearly with the binding energy in the energy range 150–500 meV. These results indicate that many-body interactions along the diagonal direction are strong down to the bottom of the band, while along the zone-boundary they become very weak at energies above 200 meV.

PACS numbers: 74.25.Gz, 74.72.Hs

Strong interactions in many-body systems lead to a rich variety of phenomena, whose understanding is a central question in modern physics. In condensed matter, cuprates are a paradigmatic example (and a continuing challenge) of the physics of strong electronic correlations. Understanding how strong interactions in cuprates affect their electronic structure is important to explain their properties, including the question of the pairing mechanism. In fact, the coupling of the carriers to elementary excitations affect the carriers' band dispersion and energy-dependent scattering rate ( $1/\tau$ ), which can be obtained respectively from the positions and widths of the spectral peaks in angle-resolved photoemission spectroscopy (ARPES) experiments [1].

In hole-doped (h-doped) cuprates,  $1/\tau$  has been mainly studied in the vicinity of the zone diagonal ( $\Phi$ ), where the superconducting (SC) gap vanishes. Here, the carriers' dispersion and scattering rate display a kink at 70 meV in the SC state [2, 3]. Beyond that energy,  $1/\tau$  increases linearly with energy in optimally doped cuprates [4]. A pressing issue in the understanding of the physics of cuprates is how the scattering rate behaves along the zone-edge (ZE), where the SC gap is maximum. An experimental difficulty in h-doped cuprates is that the band along the ZE is very shallow (about 50–100 meV), and the effects of interactions cannot be followed over a large energy range. Thus, only a few experimental reports exist, and the debate is not settled [5, 6]. In contrast, in e-doped cuprates, the ZE band-width is 500 meV, offering complete access to the momentum dependence of the many-body interactions. However, this kind of study has been scarcely addressed [7].

In this Letter we present a  $k$ -dependent study of the scattering rate in optimally doped  $\text{Sm}_{1.85}\text{Ce}_{0.15}\text{CuO}_4$  (SCCO). Compared to other e-doped cuprates, SCCO has the advantage of being cleavable, thus yielding a surface that is adequate for accurate ARPES studies. The main results are as follows. First, we find kinks in both the quasi-particle dispersion and scattering rate at 150 meV along the zone diagonal and 70 meV along the zone edge. Second, the scattering rate along the diagonal increases with an approximately linear  $1/\tau$ -dependence beyond 150 meV. In contrast, along the zone-edge the scattering rate saturates for  $1/\tau > 200$  meV. These results suggest that the electron interactions are highly anisotropic, being strong down to the bottom of the band along the diagonal, but becoming very weak beyond 200 meV along the zone-edge.

High-quality single crystalline SCCO samples were grown by a flux method and then annealed under low-oxygen pressure to render them SC with a  $T_c = 19$  K [8]. Wavelength dispersive X-ray analysis gave a Ce concentration  $x = 0.15 \pm 0.01$ . The ARPES experiments were done at the Synchrotron Radiation Center (SRC, University of Wisconsin, Madison) and the Swiss Light Source (SLS, Paul-Scherrer Institut, Switzerland) using 55 eV linear and circular photons respectively. A Scienta-2002 detector was used in both cases, with an angular resolution of 0.25°. The energy resolutions were 30 meV at SRC and 20 meV at SLS. The samples were cleaved in-situ at 11 K in pressure better than  $6 \times 10^{-11}$  Torr, and kept at these conditions during the measurements. An eventual SC gap of 1–2 meV [9] could not be resolved. The results were reproduced in three samples.

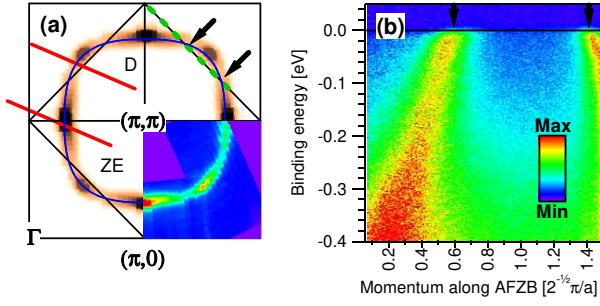


FIG. 1: (Color online) (a) FS map of SCCO samples: Data for determining the FS was taken over the first and second Brillouin zones. The spectra were integrated within 40 meV around  $E_F$ . The lower-right quadrant displays a subset of such a raw data. The rest of the figure was obtained by symmetry operations, averaging for equivalent points across the BZ diagonals, and saturating to white for intensities below 7% of the maximum intensity along the FS. The red lines indicate cuts along the ZE and D directions discussed in the text. The blue solid line is a single-band tight-binding fit to the FS. (b) D dispersion along the AFZB [green dashed line in (a)], showing the absence of antiferromagnetic-induced folding. The arrows indicate FS crossings.

We first characterize the band structure of the studied samples. Figure 1(a) shows the measured Fermi surface (FS), chosen to be centered at  $(\pi, \pi)$ . The data show a reduction of spectral weight around the crossings of the FS with the antiferromagnetic zone boundary (AFZB). The dispersion along the AFZB, shown in Fig. 1(b), shows only the bands corresponding to the barrel-like FS centered at  $(\pi, \pi)$ , indicating that no antiferromagnetic-induced folding is present [10, 11]. Such a folding has been observed only in as-grown non SC samples [10], or in underdoped reduced SC samples [12, 13]. We simultaneously fitted the FS and the high-energy part of the band-structure using a single-band tight-binding model:

$$E_{tb} = \epsilon_0 + t_1(\cos k_x + \cos k_y) + t_2(\cos k_x \cos k_y) + t_3(\cos 2k_x + \cos 2k_y); \quad (1)$$

with  $(\epsilon_0; t_1; t_2; t_3) = (-10; 590; 337; 96.6)$  meV. Such a model is a good approximation of the band-theory result [14], and our fitting parameters are close to the canonical ones [15]. The resulting FS, shown by the continuous blue line in Fig. 1(a), encloses an area corresponding to an electron-doping of  $x = 0.15 \pm 0.01$ , in agreement with the bulk nominal doping.

We now turn to the study of the many-body interactions. Within the sudden approximation, ARPES measures the occupied part of the energy and momentum ( $\mathbf{k}$ ) dependent single-particle spectral function  $A(\mathbf{k}; \omega)$  [16]:

$$A(\mathbf{k}; \omega) = \frac{1}{\omega - \epsilon_{\mathbf{k}} - \text{Re} \Sigma(\mathbf{k}; \omega) + i \text{Im} \Sigma(\mathbf{k}; \omega)}; \quad (2)$$

Here,  $\epsilon_{\mathbf{k}}$  is the bare band structure, and  $\Sigma = \text{Re} \Sigma + i \text{Im} \Sigma$

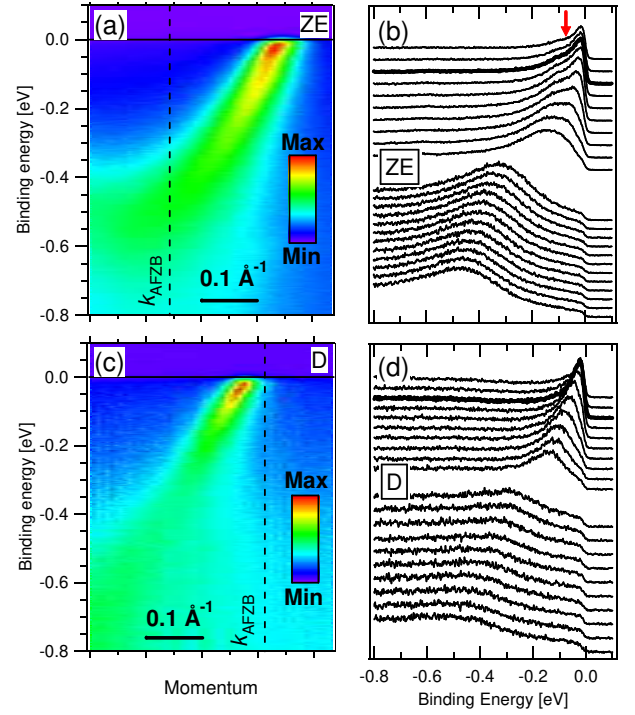


FIG. 2: (Color online) Data along the ZE (a,b) and D (c,d) directions of Fig. 1(a). The intensity maps are shown as false-color plots in (a) and (c), with the AFZB wave vectors indicated by the vertical dashed lines. EDCs near  $k_F$  and near the bottom of the band are shown in (b) and (d), with the EDCs at  $k_F$  in bold. Along the ZE, the EDCs near  $k_F$  show a peak-dip-hump structure, with the dip located at 70 meV (arrow). The line-shape of the high-energy EDCs along the ZE is approximately Lorentzian + background (see also Fig. 3). In contrast, the high-energy EDCs along the diagonal are broad and asymmetric.

is the complex self-energy (which quantifies the interactions). Energy distribution curves (EDCs) are obtained when the photoemission intensity is plotted for constant  $\mathbf{k}$ . Momentum distribution curves (MDCs) are obtained when it is plotted for constant  $\omega$ . One can obtain information about the self-energy by analyzing the EDCs and MDCs [1, 16]. Thus, if  $\Sigma$  is nearly  $\omega$ -independent for some extended energy range, then the EDCs in this energy range become Lorentzians, and their full-width at half-maximum (fwhm) is equal to  $2|\text{Im} \Sigma|$ . Likewise, an MDC is a Lorentzian if, and only if,  $\Sigma$  is independent of  $\mathbf{k}$  along the direction of the MDC and if the bare dispersion can be linearized in  $\mathbf{k}$ . It then follows from Eq. (2) that the position of the MDC peak, plotted as a function of  $\omega$ , gives the particle dispersion renormalized by interactions  $\epsilon_{\mathbf{k}}^* = \epsilon_{\mathbf{k}} + \text{Re} \Sigma$ , and the MDC-fwhm is  $\Gamma_{\mathbf{k}} = 2|\text{Im} \Sigma| = \hbar \gamma_{\mathbf{k}}$ , where  $v_{\mathbf{k}} = d\epsilon_{\mathbf{k}}/d\mathbf{k}$  is the bare-band velocity (which is experimentally unknown). Here, it is more appropriate to use the scattering rate  $\Gamma = \hbar \gamma$ , defined in terms of measurable quantities as  $\Gamma = \hbar \gamma = \hbar \text{Im} \Sigma$  ( $\gamma = \text{Im} \Sigma$ ) [17].

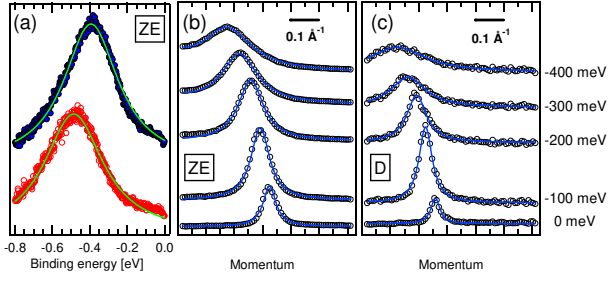


FIG. 3: (Color online) (a) Two selected EDCs along the ZE (after linear background subtraction), centered at 400 meV (filled circles) and 500 meV (open circles), and Lorentzian fits (solid lines). (b,c) Raw experimental MDCs (symbols) at selected binding energies along the ZE and D cuts, respectively, and Lorentzian fits (lines). Along the ZE, the MDCs at 300 meV were fitted with two Lorentzians of equal width, to account for the peak of the left-branch of the dispersion (outside the experimental momentum window, but close enough to the right branch to create the observed asymmetry).

Figures 2-4 show the high-statistics data and analysis along the ZE and D cuts indicated in Fig. 1(a). Along the ZE direction [Figs. 2(a,b)], the dispersion of the EDC peak can be followed down the bottom of the band, located at about 500 meV. As seen in Fig. 2(b) the EDCs at  $k_F$  along the ZE direction show a peak-dip-hump structure, with the dip located at 70 meV. For 100 & 200 meV, we find that the EDCs along this direction are well described by Lorentzians (with an approximately linear background) as shown in Fig. 3(a). All these features show that, along the ZE, the band renormalization due to interactions is strong near  $E_F$ , but becomes very weak for 100 & 200 meV, pointing to an energy-independent scattering rate, as will be confirmed further. By contrast, along the D direction, the EDCs around  $k_F$  show a single peak that broadens rapidly upon dispersing towards the bottom of the band [Fig. 2(d)]. Thus, at low energies, the coupling strength to other excitations appears to be weaker along the D than along the ZE. However, for 100 & 200 meV [Fig. 2(d)], the EDCs along the D direction become broad and asymmetric, suggesting that interactions along this direction become strong and remain energy-independent down to the bottom of the band. On the other hand, the MDCs along both directions [Figs. 3(b,c)] are Lorentzians down to 400 meV, validating the MDC analysis that follows.

Figures 4(a) and (b) show the dispersions from the peak positions of the MDCs (symbols) along the ZE and D cuts, respectively. The tight-binding band from Eq. 1 for each direction is also shown (green lines). The arrows mark the energies where the experimental dispersions are farthest from the tight-binding band, defined as the kink positions. The raw MDC widths are shown in Fig. 4(c). Along the ZE, the dispersion presents a kink

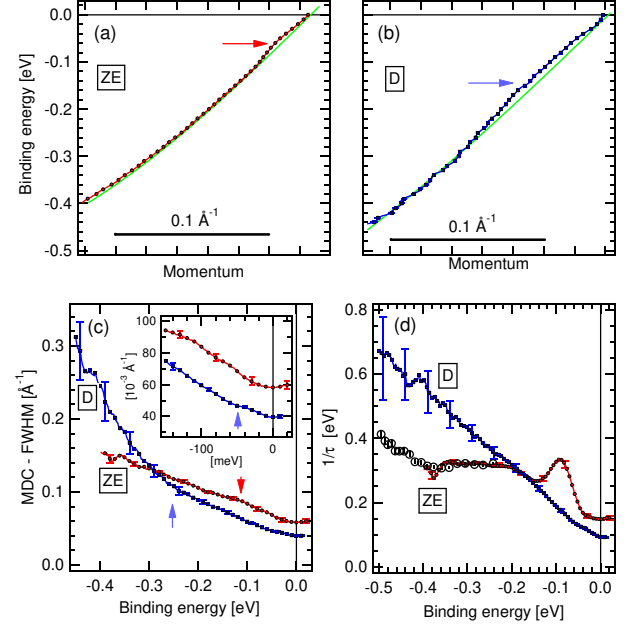


FIG. 4: (Color online) (a,b) MDC dispersions (symbols + lines) and tight-binding fits from Eq. 1 (green lines) along the ZE and D cuts, respectively. The scales are the same for comparison. (c) MDC-FWHM as a function of binding energy for the ZE and D dispersions. The inset is a zoom over the low-energy part, showing a kink at about 50 meV along D. (d) Scattering rate of the carriers (see text) along the ZE (circles) and D (squares) cuts. The open circles represent the EDC-FWHM from Lorentzian fits to the ZE data at high binding energies [Fig. 3(b)]. In all plots, the error bars represent the standard deviation from the Lorentzian fit to the peak position [Figs. (a) and (b)] and FWHM [Figs. (c) and (d)]. When not apparent, the error bars are smaller than the symbol size.

at 60-70 meV, corresponding to the dip in the EDCs near  $k_F$  [Fig. 2(b)]. A drop in the raw ZE linewidths [Fig. 4(c), full red circles] below a slightly larger energy of 100 meV is also observed, and is marked by an arrow [18]. Along the D cut, the experimental dispersion deviates from the tight-binding fit at about 30 meV, then both dispersions run almost parallel in the range 50-200 meV, and merge at 250 meV. This broad kink structure, centered at 150 meV [Fig. 4(b)], is a feature not reported before in e-doped cuprates. The raw D linewidths [Fig. 4(c), full blue squares] present a slight kink at about 50 meV (shown in the inset). At larger energies, the D linewidths increase and present an up-turn at 250 meV, about the same energy at which the D dispersion and the tight-binding band rejoin.

The scattering rates along the ZE and D directions are shown in Fig. 4(d). Along the ZE direction,  $1/\tau$  shows a peak at about 80 meV (related to the kink and drop seen in the dispersions and linewidths, respectively), while at energies larger than about 200 meV  $1/\tau$  prac-

tically saturates, indicating that the electron-scattering mechanism becomes weakly or not energy-dependent. An energy-independent self-energy implies Lorentzian EDCs, as we actually observed [Figs. 2(b) and 3(a)]. Moreover, as expected from an energy-independent self-energy, the EDC widths along the ZE in this energy range, shown by the open circles in Fig. 4(d), match very well with  $1 = \Gamma$ , which should then be close to the actual value of  $2\omega$ . Along the D direction, on the other hand, a change of slope in  $1 = \Gamma$  is seen at about 150 meV [Fig. 4(d)], while at larger energies this quantity continues to grow in an approximate linear way. This indicates that the scattering mechanisms along the D direction are energy-dependent down to at least 500 meV, in agreement with our previous discussion on the EDCs along the D cut.

We now compare our data with other ARPES data for e- and h-doped cuprates. The structures at 70 meV along the ZE and 50 meV along the D reproduce previous results on optimally doped  $\text{SCCO}$ ,  $\text{Nd}_{1.85}\text{Ce}_{0.15}\text{CuO}_4$  (NCCO), and  $\text{Eu}_{1.85}\text{Ce}_{0.15}\text{CuO}_4$ , and have been recently ascribed to electron-phonon interaction [7, 19]. At higher energies, our data along the D are in qualitative agreement with earlier data on NCCO [7] that found that  $1 = \Gamma$ , with  $\Gamma = 1$  to 1.55, in the range  $90 < \Gamma < 400$  meV. Our results complete the picture for e-doped cuprates, showing that along the ZE the interactions beyond 200 meV become weak, and the scattering rate energy-independent. As for the h-doped cuprates, a striking qualitative similarity with our data is the approximately linear form of the scattering rate along the diagonal [1, 3]. However, we do observe the bottom of the D band, so that no high-energy anomaly of the type reported in h-doped cuprates [20, 21] exists in e-doped cuprates. Note also that, in h-doped cuprates, a kink at an energy of 150 meV was recently unveiled, its physical origin being not yet clear [22]. Thus, our data suggest the existence of what could be a new form of electron coupling that is common to h- and e-doped cuprates.

Other probes in e-doped cuprates show signatures of the energy scales discussed here: infrared data on  $\text{Pr}_{2-x}\text{Ce}_x\text{CuO}_4$  at  $x = 0.13$  (0.15) show a broad drop at 200 meV (100 meV) in the optical scattering rates [23]. Local-tunneling spectroscopy data on optimally-doped  $\text{SCCO}$  show a hump at bias voltages 60–80 meV [24]. Both of these techniques are integrated over the FS. The optical response in cuprates is believed to be most sensitive to the excitations close to the diagonal, while the tunneling current is believed to be most sensitive to the  $(\pi, 0)$  regions. Thus, the infrared and tunnel results could be reinterpreted in terms of the energy scales found in our angle-resolved data.

In conclusion, among the k-space anisotropies in the carrier-dressing shown by our data, our most significant observation is that the scattering rate along the ZE saturates for binding energies larger than 200 meV, while along the D direction  $1 = \Gamma$  increases with the bind-

ing energy  $\Gamma$ , having a nearly linear  $\Gamma$ -dependence for  $\Gamma = 150$ –500 meV. These results point to the interaction of electrons with a strongly dispersive excitation with both a characteristic energy and a coupling strength to carriers that are momentum dependent, such that interactions along the diagonal are strong down to the bottom of the band, while they become very weak beyond

200 meV along the ZE. In the framework of cuprate superconductivity, two possibilities arise: either this unique scattering mechanism along the ZE is also present in the h-doped cuprates, or the strong antiferromagnetic fluctuations in e-doped cuprates separate two different regions in k-space, with a physics describing the D region that is similar in h- and e-doped cuprates, and a different picture describing the ZE region.

We acknowledge the European Union for supporting our work at the Swiss Light Source. The Synchrotron Radiation Center, University of Wisconsin-Madison, is supported by the National Science Foundation under award no. DMR-0537588. The work at the University of Maryland is supported by NSF contract DMR-0653535. Work at Ames Laboratory was supported by the Department of Energy – Basic Energy Sciences under Contract No. DE-AC02-07CH11358. AFSS thanks LPEM-CNRS for financial support.

- 
- [1] A. Damascelli, Z. X. Shen and Z. Hussain, *Rev. Mod. Phys.* 75, 473 (2003).
  - [2] A. K. Kaminski et al., *Phys. Rev. Lett.* 86, 1070 (2001).
  - [3] A. A. Kordyuk et al., *Phys. Rev. Lett.* 97, 017002 (2006).
  - [4] A. K. Kaminski et al., *Phys. Rev. B* 71, 014517 (2005).
  - [5] A. D. Gromko et al., *Phys. Rev. B* 68, 174520 (2003).
  - [6] T. Cuk et al., *Phys. Rev. Lett.* 93, 117003 (2004).
  - [7] N. P. A. M. itage et al., *Phys. Rev. B* 68, 064517 (2003).
  - [8] J. L. Peng, Z. Y. Li and R. L. Greene, *Physica C* 177, 79 (1991).
  - [9] H. Matsui et al., *Phys. Rev. Lett.* 95, 017003 (2005).
  - [10] P. Richard et al., *Phys. Rev. Lett.* 99, 157002 (2007).
  - [11] N. P. A. M. itage et al., *Phys. Rev. Lett.* 88, 257001 (2002).
  - [12] H. Matsui et al., *Phys. Rev. Lett.* 94, 047005 (2005).
  - [13] S. R. Park et al., *Phys. Rev. B* 75, 060501(R) (2007).
  - [14] O. K. Andersen, A. I. Liechtenstein, O. Jepsen and F. Paulsen, *J. Phys. Chem. Solids* 56, 1573 (1995).
  - [15] A. J. M. Illis et al., *Phys. Rev. B* 72, 224517 (2005).
  - [16] Stefan Hüfner, *Photoelectron Spectroscopy: Principles and Applications*, Third Edition, Springer-Verlag (2003).
  - [17] T. Yamasaki et al., *Phys. Rev. B* 75, 140513 (2007).
  - [18] A. "shift" towards a slightly larger binding energy of the drop in scattering rate can appear even in simple models of electron-phonon coupling, as shown for instance in C. Kirkegaard et al., *New J. Phys.* 7, 99 (2005).
  - [19] S. R. Park et al., *Phys. Rev. Lett.* 101, 117006 (2008).
  - [20] J. G. Raf et al., *Phys. Rev. Lett.* 98, 067004 (2007).
  - [21] J. Chang et al., *Phys. Rev. B* 75, 224508 (2007).
  - [22] W. Zhang et al., *Phys. Rev. Lett.* 100, 107002 (2008).
  - [23] A. Zimmers et al., *Europhys. Lett.* 70 (2), 225 (2005).
  - [24] A. Zimmers et al., *Phys. Rev. B* 76, 132505 (2007).